WORLD CONFERENCE ON TIMBER ENGINEERING 2025
BRISBANE, AUSTRALIA
Advancing Timber for the Future Built Environment

GLUED-IN ROD SPLICE CONNECTION FOR MASS TIMBER SHEAR WALLS IN A SIX-STORY SHAKE-TABLE TEST STRUCTURE

Steven Kontra [1], Andre R. Barbosa [2], Steve Pryor[3], Arijit Sinha[4], Barbara G. Simpson[5], John W. van de Lindt[6], Tanner J. Field[7], Patricio A. Uarac P.[8], Gustavo A. Araújo R.[9], Morgan McBain[10], Ludovica Pieroni[11], and Prashanna Mishra[12]

ABSTRACT: Mass timber (MT) shear walls have emerged as a viable option for use as the primary lateral force-resisting system in building structures. However, when implemented in mid- or high-rise, balloon-type construction, a single MT panel may not be long enough to span the full building height. Thus, to achieve a design intention of continuous walls, multiple panels must be stacked and vertically spliced. One promising design solution to provide adequate strength and stiffness for the splice connection involves installing glued-in rods (GiR) vertically along the axis of the panels. However, the existing body of full-scale experimental research is limited, and no testing is available to evaluate this connection's performance under dynamic earthquake loads. This paper presents the implementation of a GiR splice connection for balloon-type Mass Ply Panel (MPP) shear walls installed in a full-scale, six-story shake-table test building. A procedure for designing GiR wall splice connections is proposed and the structural response of the connection after a series of shake-table tests examined. Results from testing affirm the high strength and stiffness of the connection, validating the design approach and demonstrating structural adequacy for vertically splicing MT shear walls.

KEYWORDS: Earthquake, Glued-in Rods, Mass Ply Panel, Shake-Table Test, Shear Wall

[1] Steven Kontra, Structural Designer, KL&A Engineers and Builders, Golden, CO, USA, skontra@klaa.com

[2] Andre R. Barbosa, Civil and Construction Engineering, College of Engineering, Oregon State University, Corvallis, OR, USA, andre.barbosa@oregonstate.edu

[3] Steve Pryor, Research & Development, Simpson Strong-Tie, Pleasanton, California, United States, spryor@strongtie.com

[4] Arijit Sinha, College of Forestry, Oregon State University, Corvallis, Oregon, United States, arijit.sinha@oregonstate.edu

[5] Barbara G. Simpson, Civil and Environmental Engineering, School of Engineering & Doerr School of Sustainability, Stanford University, Stanford, CA, USA, bsimpson@stanford.edu

[6] John W. van de Lindt, Civil and Environmental Engineering, College of Engineering, Colorado State University, Fort Collins, CO, USA, jwv@colostate.edu

[7] Tanner J. Field, Civil and Construction Engineering, College of Engineering, Oregon State University, Corvallis, OR, USA, tanner.field@oregonstate.edu

[8] Patricio A. Uarac P., School of Civil and Construction Engineering, Oregon State University, Corvallis, Oregon, USA, patricio.uarac@oregonstate.edu

[9] Gustavo A. Araújo R., Civil and Environmental Engineering, Stanford University, Stanford, CA, USA, garaujor@stanford.edu

[10] Morgan McBain, Civil and Environmental Engineering, Stanford University, Stanford, CA, USA, mmcbain@stanford.edu

[11] Ludovica Pieroni, Civil, Environmental, and Geomatic Engineering, University College London, London, UK, ludovica.pieroni.20@ucl.ac.uk

[12] Prashanna Mishra, Civil and Environmental Engineering, College of Engineering, Colorado State University, Fort Collins, CO, USA, prashanna.mishra@colostate.edu

https://doi.org/10.52202/080513-0299

1 – INTRODUCTION

The demand for buildings in North America constructed with engineered mass timber (MT) products has grown sharply in the last 10 years [1]. Fueled by aesthetic intrigue, potential for sustainability, and enhanced constructability, designers have begun pushing the limits on utilizing MT for many building configurations [2].

While MT products have most typically been used as columns, beams, or more recently as floor panels, there is also the potential to use MT panels as shear walls to comprise the building's lateral force-resisting system (LFRS). These shear wall elements were initially incorporated into building codes for platform-type construction, where each individual panel would vertically span one-story segments. This configuration is not ideal for tall MT building construction, however, as the accumulated gravity loads of the shear walls bearing on the floor panels perpendicular-to-grain often govern the design [3]. An alternative approach utilizes the shear wall panels in a balloon-type configuration, where panels span continuously the full-height of the building. One primary challenge in this configuration is that a single panel cannot vertically span the full height of tall structures (typically 5 stories or more), as panel dimensions are constrained logistically by manufacturing and transportation capabilities. Thus, for incorporation into mid- or high-rise buildings, multiple panels must be stacked and vertically spliced.

Glued-in rods (GiR) are one potential design solution for this splice connection, having several merits including aesthetics, resistance to fire and corrosion, and ductility in seismic events. The structural behavior for GiR in pull-out tension and shear has been thoroughly investigated at the component level in a wide array of different setups that vary wood substrate, rod type, adhesive type, hole oversizing and connection geometry [4-13]. This body of research has yielded several general recommendations for designing GiR connections that include: a minimum suggested edge distance of 2.5 times the rod diameter (*d)*, a minimum rod spacing of 4-5*d* , a glue-line thickness of 2 mm with some testing showing adequate strength up to 4 mm [13], the preference for epoxy over other adhesives such as polyurethane and phenol resorcinol, the use of threaded rods to promote bond strength from enhanced mechanical interlocking, and the use of low-strength, mild steel rods to enhance the connection ductility [14], [15].

Recently, two component tests were performed in tension [6] and shear [16] for GiR in a Mass Ply Panel (MPP) [17] substrate to support the larger Natural Hazards Engineering Research Infrastructure (NHERI) Tallwood [18] and NHERI Converging Design (CD) [19] experimental campaigns. These component test specimens were detailed to the lower threshold of recommended values for edge distance (2*d*), rod spacing (4*d*), and glue-line thickness (3.2 mm [1/8 in]), to benchmark lower bound strength values and allow for greater flexibility for the full-scale design. Other detailing recommendations were followed including the use of threaded rods and epoxy. For shear, Grade (Gr) 36 mild steel rods were used. An available strength in LRFD and nominal (expected) strength were determined for a single GiR as 14.5 kN (3.3 kips) and 33.6 kN (7.6 kips), respectively. For pull-out tension tests, high strength rods were used such that the strength of other, brittle failure modes such as the adhesive failure at the MPP / steel interface, wood plug pull-out, splitting of the MPP, etc. could be characterized. Tests were conducted for GiR embedments of 305 mm (12 in), 508 mm (20 in), 610 mm (24 in), and 813 mm (32 in). For a 610 mm (24 in) embedment, a nominal strength of 255 kN (57.2 kips) and standard deviation of ±12.7 kN (2.86 kips) was determined.

Utilizing the collection of knowledge from previous experiments, a full-scale GiR connection was designed and implemented in the NHERI Tallwood ten-story and CD six-story shake-table test buildings. The six-story building is the focus of this work, where the GiR connection was used to vertically splice MPP wall panels to form a balloon-type MT rocking wall. The building was 20.7 m (68 ft) tall, with the first story being 4 m (13 ft) in height and subsequent story heights of 3.4 m (11 ft). The GiR splice occurred at approximately 12.2 m (40 ft) up the height of the building. This paper describes the design of the GiR connection, shake-table test setup, and an overview of results from testing.

2 – DESIGN

Design forces can be determined from a number of seismic design procedures, as allowed by the Authority Having Jurisdiction governing the building. For this analysis, estimates for peak shear and bending moments were determined from a complementary numerical model [20-21] which accounted for higher-mode force contributions [22-27]. Enveloped demands produced from several earthquake ground motion records including Northridge, Niigata, Ferndale, and Maule were analyzed. At the design earthquake (DE) shaking intensity level, the shear force and bending moment at the GiR connection were calculated as 143 kN (32 kips) and 972 kN-m (717 kip-ft), respectively. At the 1.1 Risk-targeted Maximum Considered Earthquake (MCE_R) level, demands were 194 kN (44 kips) and 1379 kN-m (1017 kip-ft), respectively.

https://doi.org/10.52202/080513-0299

Shear and bending moment capacities were determined considering different zones of GiR: an inner zone at the center of the wall with capacity to resist the sliding shear forces and two outer zones with capacity to resist bending moments.

The inner zone was composed of shorter embedment rods (herein called "shear GiR") with the same embedment that had been used for component testing [16]. Two rows of (7) shear GiR were implemented for the design, resulting in a total of (14) shear GiR accounting for the shear resistance. The available strength in LRFD for a single GiR (as determined in component testing [16]) was then multiplied by the total number of shear GiR to determine the design shear strength, as shown in Eqn. 1:

$$\phi V_n = \phi \cdot V_{rod} \cdot N \qquad (1)$$

where ϕV_n, ϕ, V_{rod}, and N represent the design shear strength, resistance factor (0.75), available strength in LRFD of a single GiR, and total quantity of shear GiR, respectively. Using this formulation, the design shear strength was calculated as 203 kN (45.6 kips), resulting in a demand / capacity ratio (D/C) = 0.96 when compared to shear demands at 1.1 MCE_R shaking intensity level. The expected shear strength of the connection was also calculated using the expected strength of a single GiR (as determined in component testing [16])—resulting in an expected shear strength of 470 kN (106 kips) (D/C = 0.41). The significant margin between the design and expected shear strength of the connection allowed for greater design confidence that the shear GiR could adequately resist demands from repeated, high-intensity testing. Both calculations conservatively neglected the longer embedment rods in the outer zones for their potential contribution to the shear capacity.

The two outer zones, designed with sufficient capacity to resist peak bending moments, were composed of longer embedment rods (herein called "flexural GiR"). These flexural GiR developed the flexural capacity of the section through an internal tension / compression force couple considering the GiR in tension and the MPP acting in compression. This capacity was calculated using a sectional analysis. The GiR at the extreme tension end were considered to reach the yield strain (ε_y), and the tensile force contribution from the GiR between the extreme tensile GiR and neutral axis were calculated from a linear strain profile. F1554, Gr 36 mild steel threaded rods were used whose yield strength (F_y) was calculated as 97 kN (21.8 kips). The compressive contribution from the MPP was calculated assuming a linear-elastic-perfectly-plastic state, with a compressive strength (f'_c) of 39.7 kPa (5.76 ksi) [17]. After several iterations of axial force equilibrium, the depth of the neutral axis was determined and used to calculate the respective contribution of MPP and each GiR. The design flexural capacity was calculated using Eqn. 2:

$$\phi M_n = \phi \cdot \sum_{i=1}^{9} \left(\frac{\varepsilon_{Ri}}{\varepsilon_y} F_{y)} + \frac{f_w c_1}{2} t_{wall} + f'_c c_2 t_{wall}\right. \qquad (2)$$

where ϕM_n represents the design flexural capacity, ϕ the resistance factor (0.9), ε_{Ri} the strain in each rod, f_w the stress in MPP at the extreme compression end, and c_1 and c_2 the length of the linear and constant strain region in the MPP. This calculation resulted in a design flexural capacity of 2379 kN-m (1754 kip-ft) (D/C = 0.58). For design conservatism, GiR on the compression side of the neutral axis were not considered nor the shear GiR for their flexural resistance. Figure 1 illustrates the sectional analysis performed. This connection was capacity-designed such that the rods (having a ductile failure mode in yielding) would be the weak link in the system. Considering a 610 mm (24") GiR embedment, the nominal strength minus one standard deviation of the brittle failure modes was determined to be 242 kN [6]—significantly greater than the yield strength of the rod. This margin helped to promote the ductile yielding of the rods as the controlling failure mechanism.

The full-scale connection design was detailed with consideration of the component testing configuration [6, 16] and recommendations from previous GiR studies [14-15]. The geometric layout of the GiR in the full-scale connection was designed for an edge distance of 2.6*d* and a rod spacing of 4*d*. The holes for each GiR were oversized by 6.4 mm (1/4 in), resulting in a glue-line thickness of 3.2 mm (1/8 in). Although slightly greater than recommended, this glue-line thickness was consistent with the component testing setup [6, 16] and allowed for greater construction tolerances for rod alignment. F1554, Gr 36, threaded, 25.4 mm (1 in) diameter rods were used for the connection, bonded to the MPP with a high-viscosity Simpson Strong-Tie CI-GV epoxy [28]. Heavy duty Simpson SDCF Screws were also added across the interface of the splice to provide reinforcing for the veneers. Figure 2 illustrates the geometric layout of GiR in the splice connection.

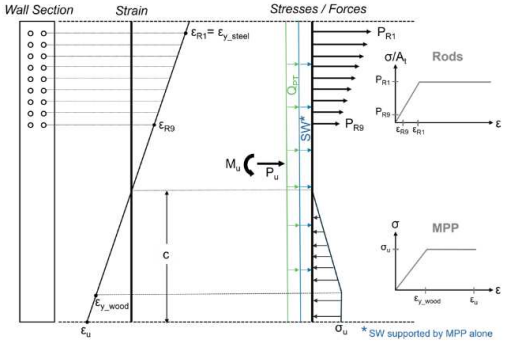

Figure 1: Sectional analysis considering flexural GiR in tension and MPP in compression, where the contribution of flexural GiR in compression are neglected.

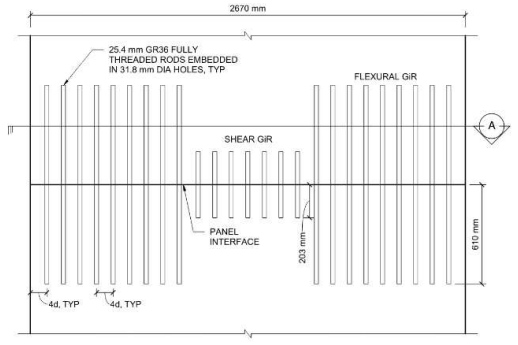

(a)

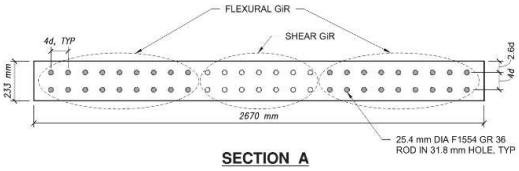

(b)

Figure 2. Geometric layout of GiR in the MPP splice connection: (a) elevation view of shear and flexural GiR located and embedments dimensioned, (b) section view with detailing requirements dimensioned.

3 – TEST PROGRAM

As previously stated, the GiR splice connection was implemented as part of the NHERI CD shake-table testing program featuring a six-story mass timber building [19]. This program consisted of three unique phases, where the LFRS in the north-south direction was exchanged for each phase. For Phase 2, notched MPP shear walls were utilized for the LFRS, with buckling-restrained boundary elements [29] vertically oriented at the base of the wall for energy dissipation and post-tensioned rods for re-centering. The rocking wall was balloon-type and composed of two stacked, vertically spliced MPP wall panels running the full-height of the building in one continuous segment. Figure 3 shows a picture from construction where the bottom MPP wall panel is in place, rods have been inserted and left loose, and the top MPP wall panel is slowly being lowered down to mate with the bottom panel as workers align rods. A more comprehensive description of the novel construction approach is described in an upcoming publication [30].

Figure 3. MPP shear wall mating: top panel slowly lowered down as loose rods are aligned.

This phase of the NHERI CD test program involved four different earthquake ground motions of varied intensity. These ground motions were scaled from 10% to 110% MCE_R and included records from the Northridge, Niigata, Ferndale, and Maule earthquakes. Table 1 shows the full suite of ground motions executed.

Table 1. Ground motion suite from Phase 2 of NHERI CD shake-table testing where X, Y, and Z represent motion in the east-west, north-south, and vertical directions, respectively.

Record ID #	Duration (s)	Test % MCE_R Intensities	Test Orientations
Northridge-01	30	10%	XYZ
			Y
		30%	Y
			XY
			XYZ
		67%	Y
			XYZ
		100%	XYZ
		110%	XYZ
Niigata, Japan	180	30%	XYZ
		67%	XYZ
		100%	XYZ
Ferndale-890	60	30%	XYZ
		67%	XYZ
		100%	XYZ
Maule Chile	90	30%	XYZ
		67%	XY
		100%	XY

The building's response to these ground motions was captured with several hundred sensors strategically placed on each story. Many different sensor types were used throughout the building, including varied

https://doi.org/10.52202/080513-0299

accelerometer models. The data for this study was sourced from triaxial accelerometers donated by ASDEA Disruptive Engineering and Technology [31]. Three ASDEA sensors were placed on each floor diaphragm at the southwest (SW) corner, center of mass (COM), and northeast (NE) corner. Figure 4 shows the location of ASDEA sensors on a typical floor plan.

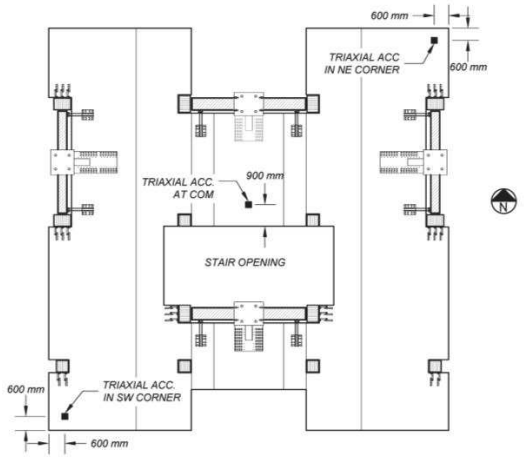

Figure 4. Typical floor plan with ASDEA accelerometers installed at the SW, NE and COM.

The data recorded from the ASDEA sensors required some post-processing to synchronize with the other sensors in the building. The data synchronization was conducted in the following steps:

(1) A time vector was created for each device using the real change in time (dt) for each time stamp (since each device recorded the time every 20 acceleration points).

(2) The device that started recording last was identified to establish the start time, and the device that stopped recording first was identified to establish the end time for synchronization across all devices.

(3) The acceleration data was interpolated across all devices so the data had a consistent time step of dt = 0.001 seconds.

Following synchronization, the acceleration response histories at each floor ($a_i(t)_{,floor}$) were cleaned with a series of steps including baseline correction, filtering, and removal of points with double-ended jerk [19]. Then, peak floor inertial forces ($F_I(t)_{floor}$) and subsequently shear and moment demands experienced by the splice during earthquake ground motions were calculated. Eqn. 3-5 show the process by which the shear and moment demands were calculated with reference to Figure 5:

$$F_I(t)_{floor} = \sum \frac{a_i(t)_{,floor}}{n_{acc}} * m_{floor} \quad (3)$$

$$V(t) = F_I(t)_{floor7} + F_I(t)_{floor6} + F_I(t)_{floor5} \quad (4)$$

$$M(t) = F_I(t)_{floor7} * \left(2h + \frac{3h}{11}\right) + F_I(t)_{floor6} * (h + \frac{3h}{11}) + F_I(t)_{floor5} * \frac{3h}{11} \quad (5)$$

where n_{acc} represents the number of accelerometers on each floor, m_{floor} the tributary mass of each floor, V(t) the shear demand with respect to time, M(t) the bending moment demand with respect to time, and h the story height.

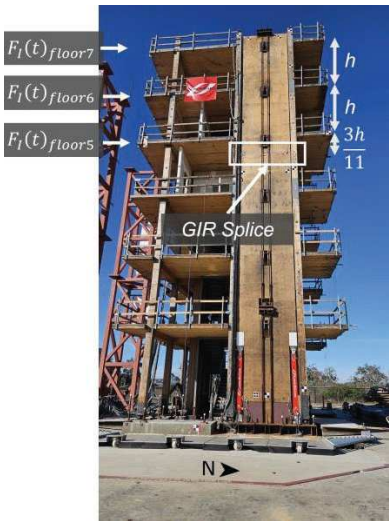

Figure 5. East elevation of shake-table test building structure with location of splice and distances of floor inertial forces with respect to the GiR splice identified.

The relative movement of the panels at the interface was also measured throughout testing. The relative panel sliding was recorded with a linear voltage displacement potentiometer (LVDT) installed horizontally at the center of the panel interface, and the edge uplift was recorded with two LVDTs installed vertically at the edges of the panel interface. Figure 6 illustrates the location of LVDTs at the panel interface.

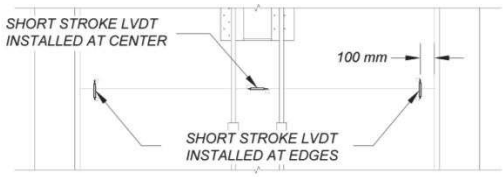

Figure 6. Elevation view of splice with LVDTs installed horizontally at the center and vertically at the edges to measure sliding and edge uplift.

4 – RESULTS

The structural response of the GiR connection was recorded for all earthquake ground motions in the NHERI CD Phase 2 test program. This paper examines the GiR performance at the DE (0.67 MCE_R) and 1.1 MCE_R shaking intensity levels for the Northridge ground motion. Results are presented in terms of the response history of shear forces and bending moments experienced by the splice considering also the relative movement of the MPP panels at the splice interface. Figure 7 summarizes results from both earthquake simulations.

At the DE intensity, the peak shear and bending moment experienced at the splice were 185 kN and 1310 kN-m (Figure 7: a, c). A comparison with the design shear and flexural strength results in a D/C of 0.91 and 0.55. Both values exceeded the expected demands but were still within the design capacity of the connection.

For the 1.1 MCE_R intensity, the peak shear and bending moment were 264 kN and 1577 kN-m (Figure 7: e, g). Comparing with the design capacity, a D/C of 1.3 and 0.66 were achieved. While the shear demands exceeded the design strength at the highest level of shaking intensity, this demand was still within the expected shear strength of the connection (470 kN).

After each round of testing, the splice was thoroughly inspected and its condition documented. However, despite the high demands exerted on the splice, relative panel movement or damage was not detected at the panel interface. These visual observations were confirmed from the recorded data measuring relative displacement at the panel interface. Figure 7b, 7d, 7f, and 7h show less than 0.2 mm of sliding or edge uplift for the duration of testing, even at the highest shaking intensity. Considering the loads experienced by the splice were higher than what was designed for, these small displacements affirm the structural competence of GiR as a high stiffness connection with significant overstrength.

6 – CONCLUSION

A GiR splice was designed to connect MPP shear wall panels in a six-story shake-table test building. The connection was designed with two different zones: one with sufficient capacity to resist the anticipated peak shear forces and the other to resist peak bending moments. During testing, the acceleration of each floor diaphragm was recorded to calculate shear and moment demands at the splice for each ground motion. At the DE shaking intensity level, peak shear and moment demands remained within the design capacity. At the 1.1 MCE_R intensity, the moment demand remained within the design capacity, while the shear demand exceeded the design capacity but remained within the expected strength of the GiR. At both levels of shaking intensity, however, very small relative movement was detected at the panel interface. Ultimately, this experiment demonstrated the high stiffness and strength of GiR connections, validating their structural adequacy for vertically splicing MT panels in tall MT building applications.

7 – ACKNOWLEDGEMENTS

This material is based upon work supported by the National Science Foundation (NSF) under awards #2120683, #2120692, and #2120684. We would also like to acknowledge the USDA Agricultural Research Service, the TallWood Design Institute, Simpson Strong-Tie, and our other industry partners [32] for supporting this experimental program. Any opinions, findings, and conclusions are those of the authors and do not necessarily reflect views of the supporting agencies.

https://doi.org/10.52202/080513-0299

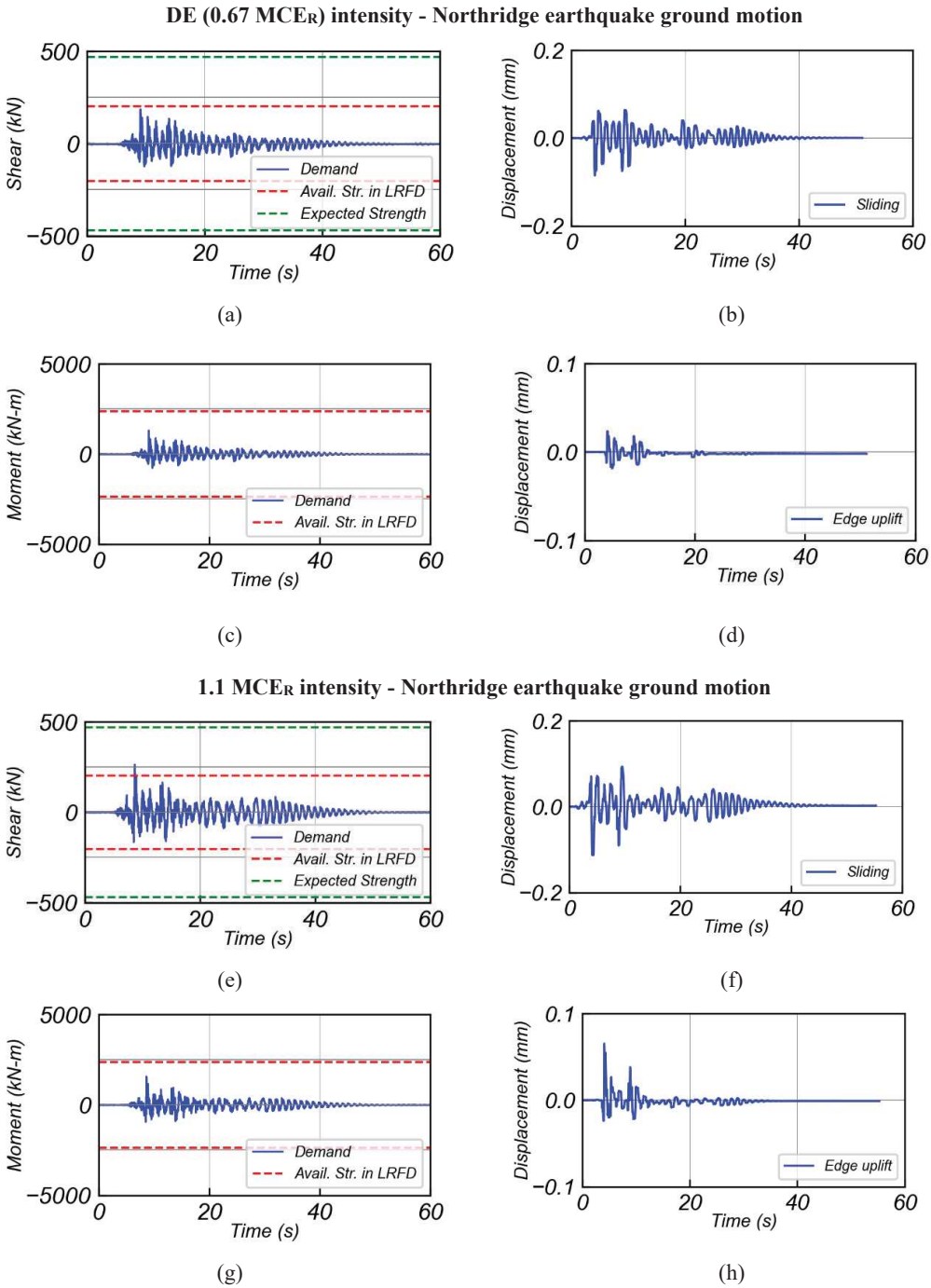

Figure 7. Results from shake-table testing using the Northridge earthquake ground motion scaled at DE (a-d) and 1.1 MCE_R (e-h) shaking intensity levels: (a, e) shear demand time history, (b, f) relative sliding at splice interface, (c, g) bending moment demand time history, (d, h) relative sliding at splice interface.

8 – REFERENCES

[1] Woodworks, "Mapping Mass Timber," The Woodworks Innovation Network (WIN). [Online]. Available: https://www.woodworks.org/resources/mapping-mass-timber/

[2] I. Kuzmanovska, E. Gasparri, D. Monne, and M. Aitchison, "Tall Timber Buildings: Emerging trends and typologies," presented at the 2018 World Conference on Timber Engineering, Seoul, Republic of Korea, Aug. 2018.

[3] Z. Chen and M. Popovski, "Mechanics-based analytical models for balloon-type cross-laminated timber (CLT) shear walls under lateral loads," *Engineering Structures*, vol. 208, p. 109916, Apr. 2020, doi: 10.1016/j.engstruct.2019.109916.

[4] K. W. Johansson, "Theory of Timber Connections," *International Association of Bridge and Structural Engineering*, vol. 9, pp. 249–262, 1949.

[5] C. Bengtsson and C.-J. Johansson, "GIROD - Glued-in Rods for Timber Structures," Swedish National Testing and Research Institute, Boras, Sweden, SMT4-CT97-2199, 2002.

[6] T. Field, A. R. Barbosa, R. B. Zimmerman, S. Pryor, A. Sinha, and C. Higgins, "Experimental and analytical evaluation of the tension capacity of edgewise connected glued-in rods in mass ply panels," *Construction and Building Materials*, vol. 409, p. 133853, Dec. 2023, doi: 10.1016/j.conbuildmat.2023.133853.

[7] J. X. Deng, "Strength of Epoxy Bonded Steel Connections in Glue Laminated Timber," University of Canterbury, 1997.

[8] R. Steiger, E. Gehri, and R. Widmann, "Pull-out strength of axially loaded steel rods bonded in glulam parallel to the grain," *Mater Struct*, vol. 40, no. 1, pp. 69–78, Jan. 2007, doi: 10.1617/s11527-006-9111-2.

[9] B.-H. Xu, D.-F. Li, Y.-H. Zhao, and A. Bouchaïr, "Load-carrying capacity of timber joints with multiple glued-in steel rods loaded parallel to grain," *Engineering Structures*, vol. 225, p. 111302, Dec. 2020, doi: 10.1016/j.engstruct.2020.111302.

[10] T. K. Bader, M. Schweigler, E. Serrano, M. Dorn, B. Enquist, and G. Hochreiner, "Integrative experimental characterization and engineering modeling of single-dowel connections in LVL," *Construction and Building Materials*, vol. 107, pp. 235–246, Mar. 2016, doi: 10.1016/j.conbuildmat.2016.01.009.

[11] G. S. Ayansola, T. Tannert, and T. Vallee, "Experimental investigations of glued-in rod connections in CLT," *Construction and Building Materials*, vol. 324, p. 126680, Mar. 2022, doi: 10.1016/j.conbuildmat.2022.126680.

[12] M. Subhani, S. K. Shill, S. Al-Deen, M. Anwar-Us-Saadat, and M. Ashraf, "Flexural Performance of Splice Connections in Cross-Laminated Timber," *Buildings*, vol. 12, no. 8, p. 1124, Jul. 2022, doi: 10.3390/buildings12081124.

[13] A. Rossignon and B. Espion, "Experimental assessment of the pull-out strength of single rods bonded in glulam parallel to the grain," *Holz Roh Werkst*, vol. 66, no. 6, pp. 419–432, Dec. 2008, doi: 10.1007/s00107-008-0263-3.

[14] R. Steiger *et al.*, "Strengthening of timber structures with glued-in rods," *Construction and Building Materials*, vol. 97, pp. 90–105, Oct. 2015, doi: 10.1016/j.conbuildmat.2015.03.097.

[15] G. Tlustochowicz, E. Serrano, and R. Steiger, "State-of-the-art review on timber connections with glued-in steel rods," *Mater Struct*, vol. 44, no. 5, pp. 997–1020, Jun. 2011, doi: 10.1617/s11527-010-9682-9.

[16] S. Kontra, A. R. Barbosa, R. B. Zimmerman, S. Pryor, C. Higgins, and A. Sinha, "Experimental Evaluation of the Interface Shear Capacity of a Mass Timber Panel Splice Connection using Glued-In Rods," *Submitted to the ASCE Journal of Materials in Civil Engineering*, 2025.

[17] ICC-ES, "ESR-4760: Freres Mass Ply Panel (MPP)," International Code Council (ICC) Evaluation Service, 2022. [Online]. Available: https://icc-es.org/report-listing/esr-4760/

[18] S. Pei *et al.*, "Shake-Table Testing of a Full-Scale 10-Story Resilient Mass Timber Building," *J. Struct. Eng.*, vol. 150, no. 12, p. 04024183, Dec. 2024, doi: 10.1061/JSENDH.STENG-13752.

[19] A. R. Barbosa *et al.*, "Shake table testing program of 6-story mass timber and hybrid resilient structures (NHERI Converging Design project)." Designsafe-CI, 2024. doi: 10.17603/DS2-RH8Q-RN95.

[20] F. McKenna, M. H. Scott, and G. L. Fenves, "Nonlinear Finite-Element Analysis Software Architecture Using Object Composition," *J. Comput. Civ. Eng.*, vol. 24, no. 1, pp. 95–107, Jan. 2010, doi: 10.1061/(ASCE)CP.1943-5487.0000002.

[21] G. A. Araujo R., "Design, Experimental Testing, and Numerical Analysis of a Three-Story Mass Timber Building with a Pivoting Spine and

https://doi.org/10.52202/080513-0299

Buckling-Restrained Energy Dissipators," Master's Thesis, Oregon State University, 2022.

[22] M. O. Eberhard and M. A. Sozen, "Behavior-Based Method to Determine Design Shear in Earthquake-Resistant Walls," *J. Struct. Eng.*, vol. 119, no. 2, pp. 619–640, Feb. 1993, doi: 10.1061/(ASCE)0733-9445(1993)119:2(619).

[23] A. Martin and G. G. Deierlein, "Generalized modified modal superposition procedure for seismic design of rocking and pivoting steel spine systems," *Journal of Constructional Steel Research*, vol. 183, p. 106745, Aug. 2021, doi: 10.1016/j.jcsr.2021.106745.

[24] M. Panagiotou and J. I. Restrepo, "Dual-plastic hinge design concept for reducing higher-mode effects on high-rise cantilever wall buildings," *Earthq Engng Struct Dyn*, vol. 38, no. 12, pp. 1359–1380, Oct. 2009, doi: 10.1002/eqe.905.

[25] M. J. N. Priestley and A. D. Amaris, "Dynamic Amplification of Seismic Moments and Shear Forces in Cantilever Walls," presented at the Concrete Structures in Seismic Regions, Athens, Greece, 2003.

[26] B. G. Simpson and D. Rivera Torres, "Simplified Modal Pushover Analysis to Estimate First- and Higher-Mode Force Demands for Design of Strongback-Braced Frames," *J. Struct. Eng.*, vol. 147, no. 12, p. 04021196, Dec. 2021, doi: 10.1061/(ASCE)ST.1943-541X.0003163.

[27] T. C. Steele and L. D. A. Wiebe, "Dynamic and equivalent static procedures for capacity design of controlled rocking steel braced frames," *Earthq Engng Struct Dyn*, vol. 45, no. 14, pp. 2349–2369, Nov. 2016, doi: 10.1002/eqe.2765.

[28] Simpson Strong-Tie, "CI-GV Gel-Viscosity Injection Epoxy: Technical Guide," Pleasanton, CA, 2023.

[29] Q. Jiang *et al.*, "Experimental study and numerical simulation of a reinforced concrete hinged wall with BRBs at the base," *Journal of Building Engineering*, vol. 49, p. 104030, May 2022, doi: 10.1016/j.jobe.2022.104030.

[30] S. Kontra *et al.*, "A Mass Timber Rocking Wall Splice Connection using Glued-in Rods: Design, Implementation, and Shake-Table Testing in a Six-Story Building," *Submitted to Engineering Structures*, 2025.

[31] *ASDEA Hardware*. (2023). [Online]. Available: https://asdea.eu/hardware/products-services/

[32] A. R. Barbosa, "NHERI Converging Design." [Online]. Available: https://tallwoodinstitute.org/nheri-converging-design/